Structure-Guided Programming of Polyketide Chain-Length Determination in Chalcone Synthase†

Joseph M. Jez, Marianne E. Bowman, and Joseph P. Noel*

Structural Biology Laboratory, The Salk Institute for Biological Studies, 10010 North Torrey Pines Road, La Jolla, California 92037

Received July 30, 2001; Revised Manuscript Received October 2, 2001

ABSTRACT: Chalcone synthase (CHS) belongs to the family of type III polyketide synthases (PKS) that catalyze formation of structurally diverse polyketides. CHS synthesizes a tetraketide by sequential condensation of three acetyl anions derived from malonyl-CoA decarboxylation to a *p*-coumaroyl moiety attached to an active site cysteine. Gly256 resides on the surface of the CHS active site that is in direct contact with the polyketide chain derived from malonyl-CoA. Thus, position 256 serves as an ideal target to probe the link between cavity volume and polyketide chain-length determination in type III PKS. Functional examination of CHS G256A, G256V, G256L, and G256F mutants reveals altered product profiles from that of wild-type CHS. With *p*-coumaroyl-CoA as a starter molecule, the G256A and G256V mutants produce notably more tetraketide lactone. Further restrictions in cavity volume such as that seen in the G256L and G256F mutants yield increasing levels of the styrylpyrone *bis*-noryangonin from a triketide intermediate. X-ray crystallographic structures of the CHS G256A, G256V, G256L, and G256F mutants establish that these substitutions reduce the size of the active site cavity without significant alterations in the conformations of the polypeptide backbones. The side chain volume of position 256 influences both the number of condensation reactions during polyketide chain extension and the conformation of the triketide and tetraketide intermediates during the cyclization reaction. These results viewed in conjunction with the natural sequence variation of residue 256 suggest that rapid diversification of product specificity without concomitant loss of substantial catalytic activity in related CHS-like enzymes can occur by site-specific evolution of side chain volume at position 256.

Polyketide synthases (PKS)[1] catalyze the biosynthesis of structurally diverse natural products from simple molecular building blocks such as thioester-linked acetate and propionate units (*1*). The diversity of polyketides in nature results from alterations in the length and chemistry of the polyketide chain. While chain-length determination is largely due to the selectivity of the particular PKS, chemical variation along the polyketide chain arises from additional modifications of the polyketide scaffold by tailoring enzymes. The type III PKS are structurally the simplest PKS (*2, 3*) while arguably the most complex PKS from a mechanistic standpoint. These enzymes function as homodimeric iterative PKS (monomer molecular mass ≈42−45 kDa) that contain two independent active sites each of which catalyzes single or multiple condensation reactions to generate polyketides of different lengths (*3*−*5*). One of the best-characterized type III PKS is chalcone synthase (CHS, EC 2.3.1.74). CHS is essential for formation of 4,2′,4′,6′-tetrahydroxychalcone (Figure 1; chalcone, **1a**), a plant secondary metabolite that sits at a critical metabolic branch point leading to the biosynthesis of anthocyanin pigments, anti-microbial phytoalexins, and flavonoid inducers of *Rhizobium* nodulation genes (*6*−*8*).

Chalcone formation by CHS begins with the transfer of a coumaroyl moiety from a *p*-coumaroyl-CoA starter molecule to an active site cysteine (*9*). Next, a series of condensation reactions, each proceeding through an acetyl-CoA carbanion derived from malonyl-CoA decarboxylation, extends the polyketide intermediate (Figure 1). Following generation of the thioester-linked tetraketide, a regiospecific intramolecular Claisen condensation forms a new ring system to yield chalcone (**1a**). Metabolically, chalcone isomerase stereospecifically converts chalcone (**1a**) to (*2S*)-5,7,4′-trihydroxyflavanone (naringenin) (Figure 1); however, spontaneous ring closure in vitro results in mixed enantiomers of naringenin (*10, 11*).

† This work was supported by a grant from the National Science Foundation (MCB9982586) to J.P.N. J.M.J. is an NIH Postdoctoral Research Fellow (CA80396) and also received support from the Hoffman Foundation.

* To whom correspondence should be addressed at The Salk Institute for Biological Studies. Phone: (858) 453-4100, ext. 1442. Fax: (858) 452-3683. E-mail: noel@sbl.salk.edu.

[1] Abbreviations: *bis*-noryangonin, 4-hydroxy-6-(4-hydroxystyryl)-2-pyrone; chalcone, 4,2′,4′,6′-tetrahydroxychalcone; CHS, chalcone synthase (EC 2.3.1.74); CoA, coenzyme A; CTAL, coumaroyltriacetic acid lactone, 4-hydroxy-6-[4-(4-hydroxyphenyl)-2-oxo-3-butenyl]-2-pyrone; DTT, D/L-dithiothreitol; HEPES, 4-(2-hydroxyethyl)-1-piperazineethanesulfonic acid; IPTG, isopropyl 1-thio-β-D-galactopyranoside; LC/MS/MS, liquid chromatography-coupled mass spectrometry; methylpyrone, 6-methyl-4-hydroxy-2-pyrone; naringenin, 5,7,4′-trihydroxyflavanone; phlorobenzophenone, phenyl-(2,4,6-trihydroxyphenyl)methanone; phlorobenzyl ketone, 2-phenyl-1-(2,4,6-trihydroxyphenyl)-ethanone; phlorohexanyl ketone, phenyl-(2,4,6-trihydroxyphenyl)hexan-1-one; NTA, nitrilotriacetic acid; PCR, polymerase chain reaction; PIPES, piperazine-*N*,*N*′-bis(2-ethanesulfonic acid); PKS, polyketide synthase; 2-PS, 2-pyrone synthase; SSRL, Stanford Synchrotron Radiation Laboratory; TLC, thin-layer chromatography.

10.1021/bi015621z CCC: $20.00
Published on Web 11/10/2001

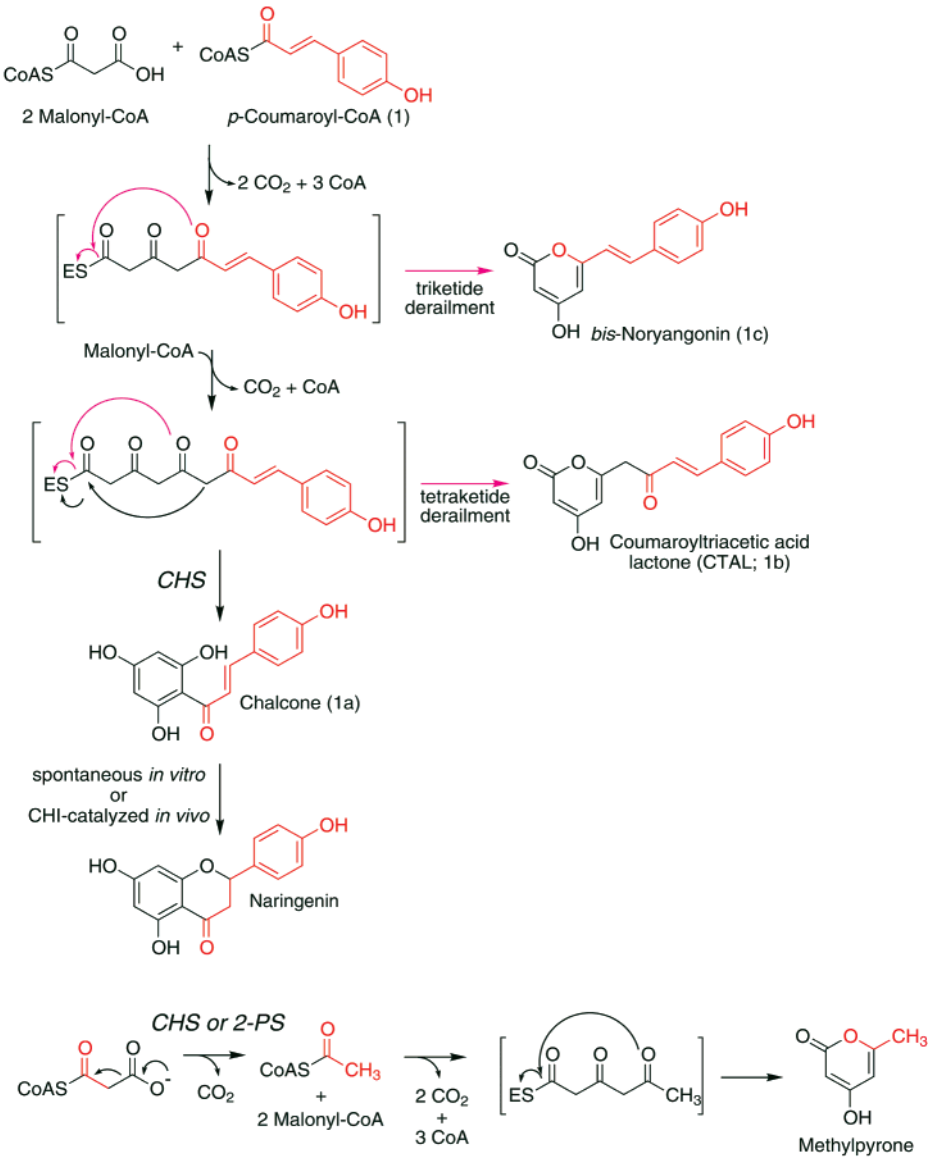

FIGURE 1: Polyketide assembly and CHS products. Chalcone formation catalyzed by CHS proceeds through an iterative series of decarboxylative condensations that extend the polyketide intermediate. The final tetraketide undergoes cyclization to chalcone, and a second cyclization in a spontaneous nonstereospecific manner leading to (2*R*/2*S*)-naringenin in vitro. In vivo, this second ring closure is stereospecifically catalyzed by chalcone isomerase (CHI), resulting in the synthesis of (2*S*)-naringenin. Derailment products of the CHS reactions, shown on the right side, include *bis*-noryangonin (formed at the triketide stage) and coumaroyltriacetic acid lactone (CTAL; produced from the tetraketide). Portions of each molecule derived from *p*-coumaroyl-CoA are indicated in red. Possible cyclization pathways to derailment products are indicated by magenta arrows. 6-Methyl-4-hydroxy-2-pyrone (methylpyrone) is formed from an acetyl-CoA starter molecule generated in situ by CHS-catalyzed decarboxylation of malonyl-CoA. This starter is then elongated by two successive acetyl-CoA α-carbanions to generate an intermediate triketide that undergoes cyclization to methylpyrone.

Structurally, the catalytic center of CHS sits at the intersection of the CoA binding site and a large internal cavity that accommodates the growing polyketide (*12*). The CoA binding site juxtaposes activated CoA-linked thioesters with the bi-lobed initiation/elongation/cyclization cavity of CHS, which contains three essential catalytic residues, namely, Cys164, His303, and Asn336 (*13*, *14*). One lobe of this cavity forms a coumaroyl binding pocket, and the other accommodates the growing polyketide chain (Figure 2). The volume and shape of the initiation/elongation/cyclization cavity govern starter molecule selectivity, polyketide chain length, and the folding and cyclization pathway of the polyketide chain in different type III PKS. For instance, *Gerbera hybrida* 2-pyrone synthase (2-PS) shares 74% amino acid identity with alfalfa CHS2 but forms a triketide from an acetyl-CoA starter and two malonyl-CoA extender units. The structure of 2-PS reveals that amino acid differences in the residues lining the active site reduce the volume of the internal cavity (*15*). Alteration of the CHS active site by introducing three amino acid substitutions, T197L, G256L, and S338I, chosen to resemble the 2-PS active site, functionally converts CHS into 2-PS (*15*).

Within the CHS initiation/elongation/cyclization cavity, the position of the Gly256 α-carbon on the active site surface abutting the elongating polyketide chain makes it an ideal target for site-directed mutagenesis aimed at testing the link between cavity volume and polyketide chain-length determination in type III PKS. The position of Gly256 in the cavity allows for the introduction of a sterically increasing set of side chains projecting into the initiation/

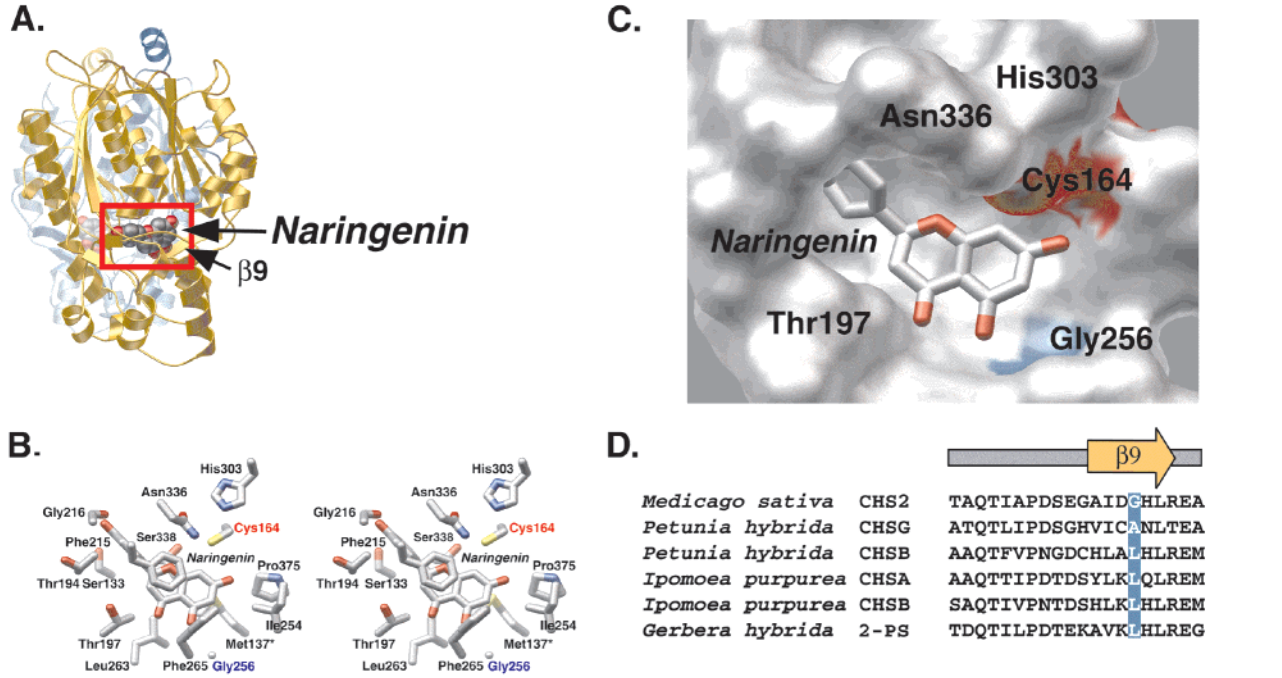

FIGURE 2: CHS initiation/elongation/cyclization cavity. (A) Ribbon diagram of CHS complexed with (2*S*)-naringenin (space-filling model) (*12*). (B) Stereoview of residues forming the active site cavity. This view is slightly rotated from that shown in (A) and is oriented looking down the CoA binding tunnel into the active site. The coumaroyl binding pocket is on the left side of the cavity. The right side of the pocket accommodates the growing polyketide chain and is the site where cyclization to chalcone occurs. (C) Surface representation of the cavity showing the complementary shape and size to naringenin. This view is oriented the same as (B). Surfaces corresponding to Phe215, Ile254, and Phe265 have been removed for clarity. The positions of Cys164 and Gly256 are indicated in red and blue, respectively. (D) Amino acid sequence alignment of the region neighboring Gly256 (CHS numbering) in CHS-related enzymes with larger side chains at this position: *Medicago sativa* CHS2 (SP: P30074), *Petunia hybrida* CHSG (PIR: SYPJCG), *Petunia hybrida* CHSB (PIR: SYPJCB), *Ipomoea purpurea* CHSA (SP: P48397), *Ipomoea purpurea* CHSB (SP: P48398), *Gerbera hybrida* 2-PS (EMB: CAA86219.1).

elongation/cyclization cavity. Although functionally characterized tetraketide-forming type III PKS, including other CHS (*16*−*20*), stilbene synthase (*20*−*22*), coumaroyltriacetic acid lactone synthase (*23*), bibenzyl synthase (*24*), homoeriodictyol/eriodictyol synthase (*25*), and acridone synthase (*26*), possess a glycine at position 256, natural variation at this position occurs in *Gerbera hybrida* 2-PS, *Petunia hybrida* CHS-B and CHS-G, and *Ipomoea* (morning glory) CHS-A and -B (Figure 2D) (*27*−*29*). The substrate and product specificities of these CHS-like proteins with the exception of 2-PS are currently unknown. Since previous experiments with the CHS G256L mutant resulted in altered product formation (*15*), we now examine in finer detail the structural and catalytic effects of incrementally changing the side chain volume of the residue at position 256 in alfalfa CHS2. The three-dimensional structures of the resulting CHS G256A, G256V, G256L, and G256F mutants reveal reductions in the volume of the active site cavity that favorably correlate with the altered product profiles of these mutants compared to wild-type CHS. This study provides a near-atomic-resolution understanding of the structural changes that result from modifying the internal active site cavity of CHS and the impact of these modifications on polyketide chain-length determination in type III PKS.

EXPERIMENTAL PROCEDURES

Materials. Oligonucleotides were ordered from Operon, Inc. The QuikChange site-directed mutagenesis kit was obtained from Stratagene. [2-^{14}C]-Malonyl-CoA (45.8 mCi/mmol) was purchased from NEN. *p*-Coumaroyl-CoA (**1**) and feruloyl-CoA (**2**) were synthesized with reagents purchased from Indofine, Aldrich, or Sigma (*29*). Electrospray mass spectrometry confirmed the identity of each product (mass spectrometry facility at The Scripps Research Institute). Malonyl-CoA, hexanoyl-CoA (**3**), phenylacetyl-CoA (**4**), and benzoyl-CoA (**5**) were obtained from Sigma. Homoeriodictyol was purchased from Indofine.

Mutagenesis, Expression, and Purification. The CHS G256A, G256V, G256L, and G256F mutants were constructed using the QuikChange method and a complementary pair of degenerate primers [5′-dGAAGGAGCCATTGATWXTCACCTTCGTGAAGCTG-3′ and 5′-dCAGCTTCACGAAGGTGAYZATCAATGGCTCCTTC-3′ (mutated codons are underlined; W = C, G, or T; X = C or T; Y = A or G; Z = A, G, or C)]. Automated nucleotide sequencing was used to select mutant genes and to confirm the fidelity of the entire CHS gene (Salk Institute DNA Sequencing Facility). Recombinant proteins were overexpressed in *E. coli* BL21(DE3) cells using the pHIS8 vector and were purified to homogeneity, as described previously (*13*).

Enzyme Assays. CHS activity was determined by measuring the conversion of *p*-coumaroyl-CoA (**1**) and [2-^{14}C]-malonyl-CoA into reaction products (*13*). Reactions were quenched with 5% (v/v) acetic acid and extracted with ethyl acetate. Percent product yields for each mutant were determined by scraping the thin-layer chromatography (TLC) plate and quantifying the radioactivity in each spot using scintillation counting. Reactions with feruloyl-CoA (**2**), hexanoyl-CoA (**3**), phenylacetyl-CoA (**4**), and benzoyl-CoA (**5**) were performed in an analogous manner to the *p*-coumaroyl-CoA assays described above. Kinetic constants were determined from initial velocity measurements, in which product forma-

tion was linear over the time periods monitored (1−10 min), using standard assay conditions (2−10 μg of protein, 100 mM potassium phosphate buffer, pH 7.0, 100 μL reaction volume at 25 °C) with either 71 μM malonyl-CoA (100 000 cpm) and varied starter molecule concentrations (0.5−50 μM) or 50 μM starter molecule and varied malonyl-CoA concentrations (2.1−71 μM; 10 000−100 000 cpm). Data were fit to the Michaelis−Menten equation using KaleidaGraph (Synergy Software).

Liquid Chromatography-Coupled Mass Spectrometry (LC/MS/MS) Product Analysis. Scaled-up assays (5 mL reaction volume; 100 μg of protein) were performed under standard assay conditions with 50 mM 4-(2-hydroxyethyl)-1-piperazineethanesulfonic acid (HEPES, pH 7.0) instead of potassium phosphate buffer. All reactions used 50 μM starter molecule [*p*-coumaroyl-CoA (**1**), feruloyl-CoA (**2**), hexanoyl-CoA (**3**), phenylacetyl-CoA (**4**), or benzoyl-CoA (**5**)] and 120 μM malonyl-CoA as the extender molecule. Reactions were quenched with 5% (v/v) acetic acid and extracted with ethyl acetate. Product analysis was performed at the mass spectrometry facility at The Scripps Research Institute. Extracts were analyzed on a Hewlett-Packard HP1100 MSD single quadrupole mass spectrometer coupled to a TSK-Gel ODS-80TS (TosoHaas) column (5 μm, 4.6 mm × 150 mm). HPLC conditions were as follows: gradient system from 30 to 70% (v/v) methanol in water [each containing 0.2% (v/v) acetic acid] within 30 min; flow rate 0.8 mL/min. The LC/MS/MS data are presented below. All numbers show *m*/*z* values in atomic mass units with relative intensities in parentheses. Fragmentation data for each compound match previously determined patterns (*15*, *31*). Products of *p*-coumaroyl-CoA (**1**) reactions: naringenin, $[M-H]^-$ 271 (100), $[M-H-CO_2]^-$ 227 (18), 203 (3), 151 (49), 119 (58); CTAL (*p*-coumaroyltriacetic acid lactone, **1b**), $[M-H]^-$ 271 (100), $[M-H-CO_2]^-$ 227 (15), 203 (25), $[M-H-CO_2-CH_2-CO]^-$ 185 (21), 161 (41), 145 (57), 125 (32), 119 (15); bis-noryangonin (**1c**), $[M-H]^-$ 229 (100), $[M-H-CO_2]^-$ 185 (17), $[M-H-CO_2-CH_2CO]^-$ 143 (25); methylpyrone (6-methyl-4-hydroxy-2-pyrone), $[M-H]^-$ 125 (100), $[M-H-CO_2]^-$ 81 (74). Products of feruloyl-CoA (**2**) reactions: compound **2b**, $[M-H]^-$ 301 (100), $[M-H-CO_2]^-$ 257 (10), $[M-H-CO_2-CH_2]^-$ 243 (21), $[M-H-CO_2-CH_2-CO]^-$ 215 (28), 191 (38), 175 (75); compound **2c**, $[M-H]^-$ 259 (100), $[M-H-CO_2]^-$ 215 (23), $[M-H-CO_2-CH_2]^-$ 201 (55), $[M-H-CO_2-CH_2-CO]^-$ 173 (62). Products of hexanoyl-CoA (**3**) reactions: compound **3b**, $[M-H]^-$ 223 (100), $[M-H-CO_2]^-$ 179 (12), $[M-H-CO_2-CH_2-CH_2]^-$ 151 (18), $[M-H-CO_2-CH_2-CH_2-CH_2]^-$ 137 (29), 125 (35); compound **3c**, $[M-H]^-$ 181 (100), $[M-H-CO_2]^-$ 137 (97), 97 (23). Products of phenylacetyl-CoA (**4**) reactions: phlorobenzyl ketone (**4a**), $[M-H]^-$ 243 (100), 227 (38), 203 (21), 161 (12), 91 (27); compound **4b**, $[M-H]^-$ 243 (100), $[M-H-CO_2]^-$ 199 (20), 151 (61), 157 (10), 125 (58), 117 (12), 107 (35); compound **4c**, $[M-H]^-$ 201 (100), $[M-H-CO_2]^-$ 157 (26), 115 (10), 91 (32). Products of benzoyl-CoA (**5**) reactions: phlorobenzophenone (**5a**), $[M-H]^-$ 229 (100), $[M-H-CO_2]^-$ 185 (25), 171 (5), 153 (42); compound **5b**, $[M-H]^-$ 229 (100), $[M-H-CO_2]^-$ 185 (5), 161 (5), 143 (24), 119 (54); compound **5c**, $[M-H]^-$ 187 (100), $[M-H-CO_2]^-$ 143 (17), 115 (6), 101 (11).

Crystallization, Data Collection, and Structure Determination. Crystals of the CHS G256A, G256V, G256L, and G256F mutants were grown by vapor diffusion in hanging drops [1:1 mixture of 25 mg/mL protein and 2.2−2.4 M ammonium sulfate, 0.1 M piperazine-*N*,*N*′-bis(2-ethanesulfonic acid) (PIPES), pH 6.5, and 5 mM dithiothreitol (DTT)] at 4 °C. Diffraction data were collected for each mutant from a single-crystal mounted in a cryo-loop and flash-frozen in a nitrogen stream at 105 K. Data for the G256A and G256V mutants were collected at beamline 9-2 of the Stanford Synchrotron Radiation Laboratory (SSRL 9-2) on a Quantum 4 CCD detector. Data for the G256L mutant were collected at SSRL 7-1 on a 30 cm MAR imaging plate detector. Data for the G256F mutant were collected in the Structural Biology Laboratory at the Salk Institute for Biological Studies using a DIP2030 imaging plate system (Mac-Science Corp.) and Cu Kα radiation produced by a rotating anode operated at 45 kV and 100 mA and equipped with double-focusing Pt/Ni-coated mirrors. All images were indexed and integrated using DENZO (*32*) and the reflections merged with SCALEPACK (*32*). Data reduction was completed using programs in CCP4 (*33*) (Table 1). Structures were determined by the difference Fourier method (*34*, *35*). Wild-type CHS, with a glycine at position 256, comprised the starting model. Refinement of the protein model was conducted with REFMAC (*36*) and ARP (*37*). Inspection of the $|2F_o-F_c|$ and $|F_o-F_c|$ electron density maps and model building were performed with O (*38*). After an initial round of refinement, the difference density maps clearly showed the expected mutations and enabled the side chains to be unequivocally incorporated into each model. Successive iterations of refinement using REFMAC/ARP and model building in O were performed with refinement converging to the final *R*-factors shown in Table 1. Model quality was checked with PROCHECK (*39*).

Table 1: Data Collection and Refinement Statistics for the CHS G256A, G256V, G256L, and G256F Mutant Structures

	G256A	G256V	G256L	G256F
space group	$P3_221$	$P3_121$	$P3_121$	$P3_121$
unit cell dimensions (Å)	$a = 98.10$, $c = 65.07$	$a = 98.29$, $c = 129.7$	$a = 98.10$, $c = 131.10$	$a = 97.96$, $c = 130.3$
wavelength (Å)	1.00	1.01	1.08	1.54
resolution (Å)	39.2−1.50	46.0−1.45	31.2−1.86	23.7−1.95
total reflections	383046	1366179	390574	376124
unique reflections	53301	128367	57245	51488
completeness[a] (%)	91.4 (57.3)	99.3 (95.9)	97.3 (85.0)	97.5 (99.2)
I/σ[a]	29.7 (2.4)	29.7 (2.7)	21.9 (5.7)	14.7 (2.1)
R_{sym}[a,b]	3.9 (37.3)	4.5 (51.0)	4.2 (14.5)	5.1 (36.0)
R_{cryst}[c]/R_{free}[d] (%)	18.5/22.1	19.7/22.1	20.6/25.9	19.5/25.1
protein atoms	2996	5994	5982	5986
sulfate atoms	5	10	−	−
water molecules	404	752	450	399
rmsd bond lengths (Å)	0.019	0.020	0.021	0.022
rmsd bond angles (deg)	1.8	1.8	1.9	2.0
av *B*-factor, protein (Å^2)	20.3	18.2	23.6	28.1
av *B*-factor, solvent (Å^2)	31.4	27.2	26.7	31.1

[a] Number in parentheses is for the highest resolution shell. [b] $R_{sym} = \sum|I_h - \langle I_h\rangle|/\sum I_h$, where $\langle I_h\rangle$ is the average intensity over symmetry-equivalent reflections. [c] R_{cryst}-factor $= \sum|F_{obs} - F_{calc}|/\sum F_{obs}$, where summation is over the data used for refinement. [d] R_{free}-factor is the same definition as for *R*-factor, but includes only 5% of data excluded from refinement.

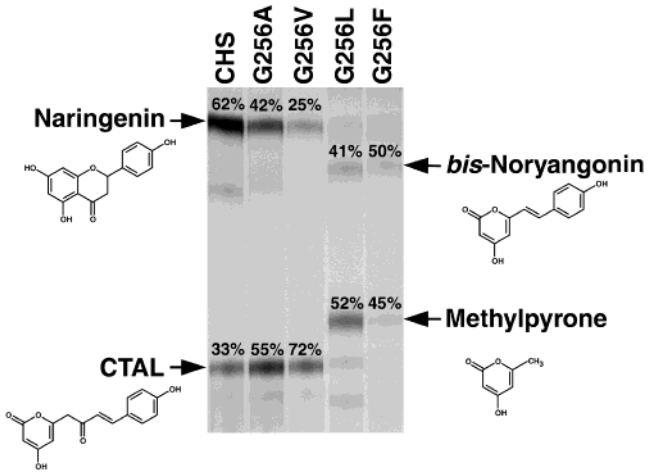

FIGURE 3: Product profiles of wild-type CHS and the Gly256 mutants using *p*-coumaroyl-CoA. Using the conditions for the standard CHS assay, as described under Experimental Procedures, the reaction products for each protein were observed by autoradiography of the TLC plate and were confirmed by LC/MS/MS analysis. The positions and chemical structures of naringenin, coumaroyltriacetic acid lactone (CTAL), *bis*-noryangonin, and methylpyrone are indicated. The percentages of each product formed are shown above each band on the TLC plate. Minor components contribute less than 5% to the total extractable products.

Calculations of cavity volumes were performed with GRASP (*40*). All structure illustrations were prepared with MOLSCRIPT (*41*) or GRASP and were rendered with POV−Ray (*42*). Atomic coordinates and structure factors for the CHS G256A, G256V, G256L, and G256F mutant structures have been deposited in the Protein DataBank under accession numbers 1I86, 1I88, 1I89, and 1I8B, respectively.

RESULTS

CHS Mutant Expression and Purification. The Gly256 series of mutants (G256A, G256V, G256L, and G256F) and structure/function characterization of the mutant proteins established the effect of increasing residue size at position 256 on polyketide chain-length determination catalyzed by CHS. CHS mutants were expressed in *E. coli* and purified to homogeneity as determined by SDS−PAGE (not shown). All of the purified proteins migrated on SDS−PAGE with a monomeric molecular mass of 42 kDa and eluted from the gel filtration column as an 85 kDa dimer (not shown). Typical yields were 5−10 mg of pure protein per liter of culture.

Screening CHS Activity with p-Coumaroyl-CoA. Wild-type CHS and the Gly256 mutants were incubated with *p*-coumaroyl-CoA (**1**) and radiolabeled malonyl-CoA. Following extraction, the reaction products of each assay were analyzed by TLC (Figure 3). Wild-type CHS yields naringenin (62% of the reaction products), which is derived nonenzymatically from chalcone (**1a**). Formation of 4-hydroxy-6-[4-(4-hydroxyphenyl)-2-oxo-3-butenyl]-2-pyrone or coumaroyltriacetic acid lactone (CTAL; **1b**) accounts for 33% of the wild-type reaction products. Mutation of Gly 256 into an alanine or a valine shifts the nargingenin:CTAL ratio to 42%:55% and 25%:72%, respectively. These mutations alter the regiospecific cyclization reaction that likely occurs near position 256.

The G256L and G256F mutant product profiles differ from wild-type CHS and the G256A and G256V mutants. Previous examination of the CHS G256L mutant demonstrated that this enzyme produces 6-methyl-4-hydroxy-2-pyrone (methylpyrone) from acetyl-CoA and two malonyl-CoAs or three malonyl-CoAs (*15*). Consistent with this observation, methylpyrone, resulting from the condensation of three malonyl-CoA molecules, is a major (52%) reaction product (Figure 3). The other major G256L product (41%) is 4-hydroxy-6-(4-hydroxystyryl)-2-pyrone or *bis*-noryangonin (**1c**), as verified by LC/MS/MS analysis. Although the G256F mutant is clearly less active than the G256L mutant, the G256F mutant exhibits a similar product distribution (50% *bis*-noryangonin; 45% methylpyrone). Minor components account for less than 5% of the total observed products by TLC analysis. Under the assay conditions used, no accumulation of methylpyrone or *bis*-noryangonin was observed with wild-type CHS or the G256A and G256V mutants.

Steady-State Kinetic Analysis of the Gly256 Mutants with Natural Substrates. To assess the quantitative effect of mutations at position 256, the steady-state kinetic parameters of wild-type CHS and the Gly256 mutants for *p*-coumaroyl-CoA and malonyl-CoA were determined (Table 2). The G256A mutant was kinetically similar to wild-type CHS. Substitution of a valine for Gly256 results in 3- and 8-fold reductions in k_{cat} values for *p*-coumaroyl-CoA and malonyl-CoA, respectively. The G256L and G256F mutants exhibit the largest changes in the steady-state kinetic parameters. The G256L mutant exhibits 75- and 9-fold reductions in catalytic efficiency (k_{cat}/K_m) with malonyl-CoA and *p*-coumaroyl-CoA, respectively. Mutation of Gly256 into a phenylalanine also reduces the catalytic efficiencies with *p*-coumaroyl-CoA and malonyl-CoA by 14- and 47-fold, respectively. These results demonstrate that introduction of larger side chains at position 256 reduces the catalytic efficiency of each mutant enzyme compared to wild-type CHS, with the most pronounced effect seen for malonyl-CoA.

Activities of the Gly256 Mutants Using Alternate Starter Molecules. Although *p*-coumaroyl-CoA is the in vivo substrate of alfalfa CHS, the enzyme will accept different CoA-linked thioesters as alternate starter molecules to generate the corresponding chalcone, tetraketide lactone, and triketide lactone products (Figure 4) (*43*, *44*). The product profiles (Figure 5) and steady-state kinetic parameters (Table 2) of wild-type CHS and the Gly256 mutants were determined using feruloyl-CoA (**2**), hexanoyl-CoA (**3**), phenylacetyl-CoA (**4**), and benzoyl-CoA (**5**) starter molecules.

Alfalfa CHS2, like parsley CHS (*43*), accepts feruloyl-CoA as a starter molecule with a 5-fold reduction in k_{cat}/K_m but does not produce the flavanone homoeriodictyol via the chalcone cyclization reaction and nonspecific ring closure to a flavanone, as confirmed by TLC and LC/MS/MS analysis. Instead wild-type CHS produces the tetraketide lactone **2b** and methylpyrone as the major products with the triketide lactone **2c** generated as a minor product, using this larger starter molecule. The acetyl-CoA used for methypyrone synthesis comes from CHS-catalyzed malonyl-CoA decarboxylation. Since feruloyl-CoA is a less efficient starter than coumaroyl-CoA, acetyl-CoA builds up due to the longer incubation times necessary to obtain detectable levels of polyketide products. Conversely, when coumaroyl-CoA and malonyl-CoA are used with wild-type CHS, the reaction is rapid and highly selective so acetyl-CoA never accumulates

Table 2: Steady-State Kinetic Constants of Wild-Type and Mutant CHS[a]

	p-coumaroyl-CoA			malonyl-CoA		
	k_{cat} (min^{-1})	K_m (μM)	k_{cat}/K_m ($s^{-1} M^{-1}$)	k_{cat} (min^{-1})	K_m (μM)	k_{cat}/K_m ($s^{-1} M^{-1}$)
CHS	5.14 ± 0.30	6.1 ± 1.3	14043	4.58 ± 0.24	4.7 ± 1.1	16241
G256A	5.48 ± 0.40	5.7 ± 1.5	16023	2.41 ± 0.20	5.1 ± 1.9	7876
G256V	1.53 ± 0.08	4.2 ± 0.8	6071	0.64 ± 0.15	4.5 ± 0.5	2370
G256L	1.06 ± 0.13	11.8 ± 3.4	1497	0.32 ± 0.05	24.5 ± 3.2	217
G256F	0.62 ± 0.02	10.6 ± 0.9	975	0.21 ± 0.09	10.2 ± 1.5	343
	feruloyl-CoA			hexanoyl-CoA		
	k_{cat} (min^{-1})	K_m (μM)	k_{cat}/K_m ($s^{-1} M^{-1}$)	k_{cat} (min^{-1})	K_m (μM)	k_{cat}/K_m ($s^{-1} M^{-1}$)
CHS	1.04 ± 0.17	5.2 ± 0.9	3333	2.52 ± 0.22	4.1 ± 1.2	10243
G256A	0.89 ± 0.17	5.5 ± 0.6	2697	2.04 ± 0.14	5.3 ± 1.2	6415
G256V	0.64 ± 0.09	5.8 ± 0.6	1839	3.03 ± 0.21	5.7 ± 1.4	8869
G256L	0.56 ± 0.09	5.3 ± 1.2	1761	1.93 ± 0.08	6.1 ± 0.6	5237
G256F	0.16 ± 0.01	5.9 ± 0.5	452	0.19 ± 0.01	6.7 ± 1.1	473
	phenylacetyl-CoA			benzoyl-CoA		
	k_{cat} (min^{-1})	K_m (μM)	k_{cat}/K_m ($s^{-1} M^{-1}$)	k_{cat} (min^{-1})	K_m (μM)	k_{cat}/K_m ($s^{-1} M^{-1}$)
CHS	2.17 ± 0.35	5.1 ± 0.7	7092	1.73 ± 0.21	2.2 ± 0.2	13106
G256A	2.41 ± 0.25	5.2 ± 0.6	7724	1.11 ± 0.13	2.3 ± 0.3	8043
G256V	1.42 ± 0.11	5.2 ± 0.9	4551	1.65 ± 0.09	2.9 ± 0.4	9821
G256L	0.66 ± 0.04	4.3 ± 1.0	2558	0.73 ± 0.09	7.3 ± 1.2	1667
G256F	0.20 ± 0.01	4.4 ± 0.8	758	0.13 ± 0.01	6.1 ± 0.4	355

[a] All reactions were performed using the radiometric assay described under Experimental Procedures. All k_{cat} and K_m values are expressed as a mean ± SE for an $n = 3$ for all products formed in each reaction.

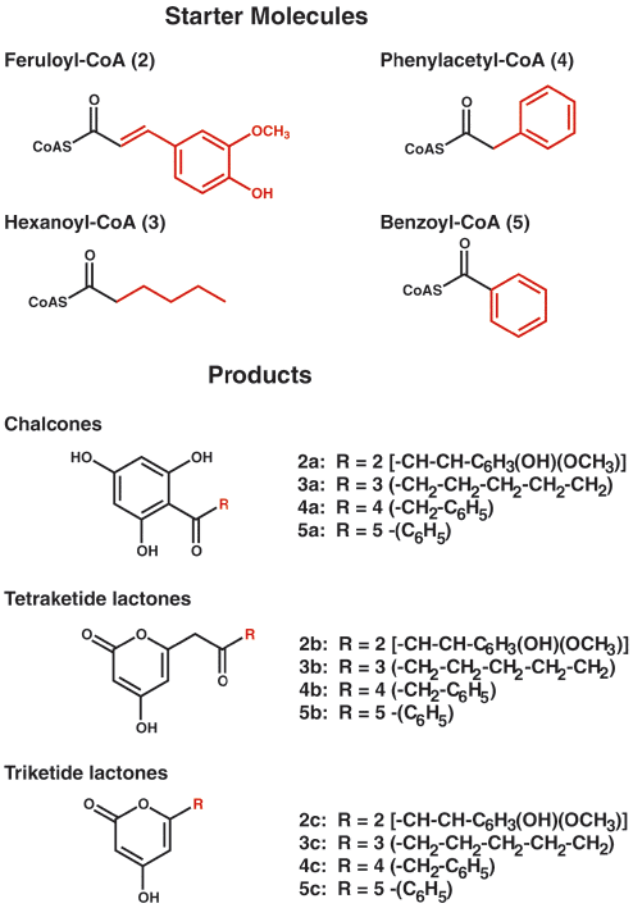

FIGURE 4: Alternate starter molecules and their predicted reaction products.

to levels sufficient to initiate methylpyrone synthesis. As bulkier side chains replace Gly256, the catalytic efficiency of each mutant CHS decreases, and the triketide lactone **2c** becomes the predominant product.

With hexanoyl-CoA, wild-type CHS does not generate phlorohexanoyl ketone (**3a**) but yields the corresponding tetraketide lactone **3b** as the major product with a k_{cat}/K_m comparable to that of *p*-coumaroyl-CoA. The triketide lactone **3c** and methylpyrone are lesser products of the wild-type reaction with this starter molecule. Interestingly, the G256A, G256V, and G256L mutants all produce similar amounts of the compound **3b** with slight reductions in catalytic efficiency. Mutation of Gly256 to a phenylalanine drastically reduces the catalytic efficiency with hexanoyl-CoA.

Wild-type CHS accepts phenylacetyl-CoA as a starter molecule. Phlorobenzyl ketone (**4a**), the chalcone-like product, accounts for less than 10% of the observed products. The tetraketide lactone **4b**, triketide lactone **4c**, and methylpyrone comprise the remaining products. The overall product distribution with phenylacetyl-CoA is similar to that reported for CHS from *Scutellaria baicalensis* (*31*). None of the Gly256 mutants yielded the chalcone-like product, indicating a complete derailment of the cyclization reaction. The Gly256 mutants yield the corresponding tetraketide lactone **4b** and triketide lactone **4c** with the triketide as the main product in the G256L and G256F mutants.

With benzoyl-CoA as the starter molecule, alfalfa CHS2 generates phlorobenzophenone (**5a**) as the major product and compounds **5b** and **5c** as minor products. Based on the observed product profiles, substitution of either an alanine or a valine at position 256 does not significantly alter the cyclization reaction of the tetraketide intermediate; however, the G256L mutant mainly yields the triketide lactone **5c**. The G256F mutant displays the lowest catalytic efficiency with this starter molecule.

Structural Analysis of the Gly256 Mutants. The observed product profiles and steady-state kinetic parameters of the Gly256 mutants indicate that increasing amino acid side chain volume at position 256 in the initiation/elongation/cyclization cavity alters the kinetic behavior and the product

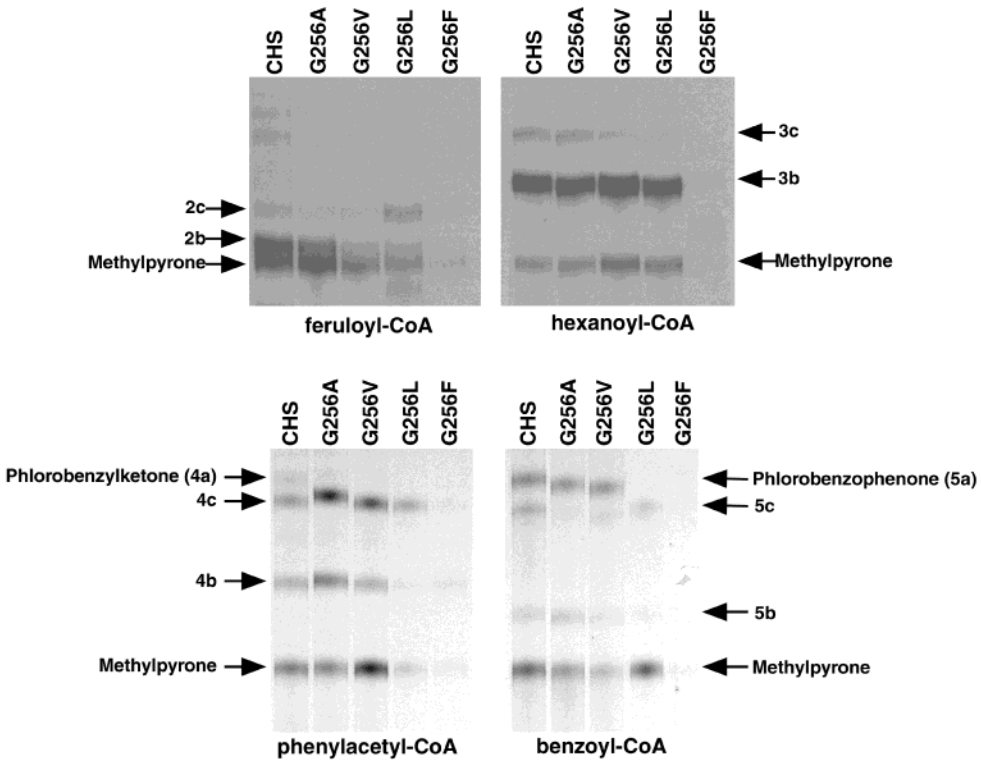

FIGURE 5: Product profiles of wild-type CHS and the Gly256 mutants using alternate starter molecules. Wild-type and mutant CHS enzymes were incubated with radiolabeled malonyl-CoA and either feruloyl-CoA, hexanoyl-CoA, phenylacetyl-CoA, or benzoyl-CoA, as described under Experimental Procedures. The reaction products for each protein were observed by autoradiography of the TLC plate and were confirmed by LC/MS/MS analysis. The position of each product is indicated. The chemical identity of each band is shown in Figure 4. Accurate quantification of product ratios is hampered by contrast adjustments necessary to visualize all products produced.

distributions in the Gly256 mutants. To correlate potential structural changes with the functional behavior of each mutant protein, the three-dimensional structures of the CHS G256A, G256V, G256L, and G256F mutants were determined by X-ray crystallography (Table 1). In the initial $|2F_o-F_c|$ and $|F_o-F_c|$ electron density maps of each structure, electron density for the substituted side chain at position 256 was unambiguous and allowed for modeling of the new side chain into each structure. Substitutions of Gly256 do not alter the overall three-dimensional structure of CHS. The rms deviations of the C_α-atoms for the G256A, G256V, G256L, and G256F mutants were 0.14 , 0.22, 0.17, and 0.18 Å, respectively, compared to wild-type CHS.

As expected from the low rms deviations, the active site structure of each Gly256 mutant is similar to that of the wild-type enzyme with the exception of the side chain of the substituted residues, which project into the portion of the active site cavity, that accommodates the growing polyketide chain (Figure 6). Specifically, the respective side chains at position 256 point into the elongation/cyclization lobe, filling the space residing next to Phe265. Previous CHS structures demonstrated that Phe265 assumes distinct conformations, adopting either the orientation observed in this current study or a second conformation that positions the phenyl moiety in the elongation/cyclization site (*12, 13*). van der Waals contacts between the substituted side chains at position 256 and Phe265 orient Phe265's aromatic ring at the intersection of the CoA binding tunnel and the entrance to the initiation/elongation/cyclization cavity. Importantly, these mutations reduce the size of the elongation/cyclization site within the broader active site cavity.

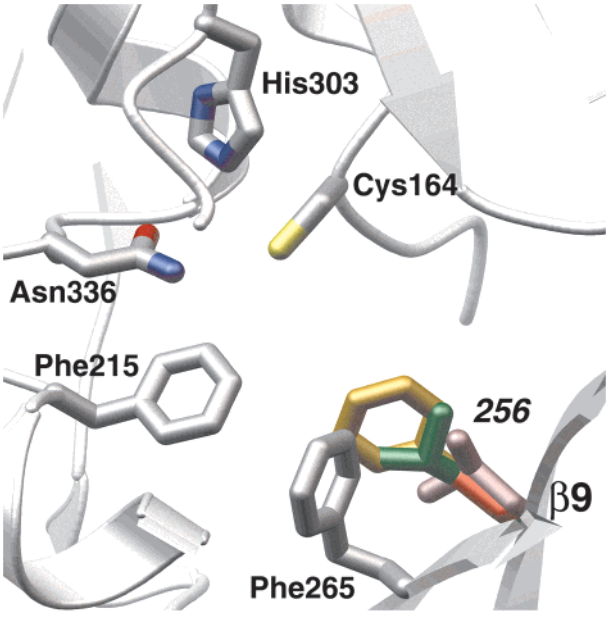

FIGURE 6: Structures of wild-type CHS and the Gly256 mutants. Since the polypeptide backbone and side chains of the residues lining the initiation/elongation/cyclization cavity are similar in each structure, only the secondary structure and selected residues of wild-type CHS (Cys164, Phe215, Gly256, Phe265, His303, and Asn336) are shown. The side chains at position 256 for each mutant are also shown (G256A, red; G256V, purple; G256L, green; G256F, gold).

Comparisons of the molecular surfaces of the initiation/elongation/cyclization cavities of wild-type CHS and the Gly256 mutants further emphasize the structural differences resulting from mutations at position 256 (Figure 7). As shown

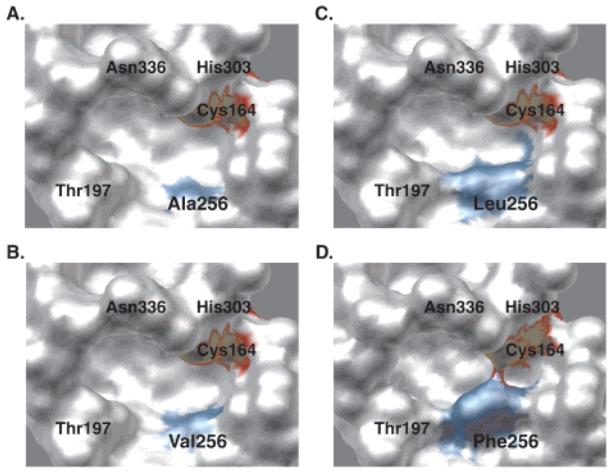

FIGURE 7: Size comparison of the initiation/elongation/cyclization cavities of the Gly256 mutants. Surface representations of the (A) G256A, (B) G256V, (C) G256L, and (D) G256F mutants are oriented the same as the view in Figure 2C and includes the same residues. The positions of Cys164 (red) and the mutated residue at position 256 (blue) are indicated.

in Figure 2C, the structure of wild-type CHS complexed with naringenin established that the active site cavity (volume = 605 Å^3) readily accommodates the product analogue, naringenin (*12*). It should be noted that this active site volume calculation for wild-type CHS differs from previously reported values due to the implementation of a more restrictive probe radius and confinement of the calculation to only the initiation/elongation/cyclization cavity.

In the wild-type CHS·naringenin complex, the coumaroyl- and malonyl-derived portions of the product are bound in different lobes of the active site cavity (*12*). In the structures of the G256A, G256V, G256L, and G256F mutants, the respective side chains at position 256 extend into the elongation/cyclization pocket of the active site cavity. This portion of the cavity was proposed to accommodate the lengthening polyketide chain, leading to formation of an acyclic tetraketide intermediate, and to promote the Claisen condensation necessary for cyclization and chalcone release.

Substitution of an alanine for Gly256 reduces the cavity volume to 601 Å^3 and produces a slight perturbation on the surface of the active site cavity (Figure 7A). The G256V mutant further shrinks the volume of the initiation/elongation/cyclization cavity to 590 Å^3 (Figure 7B). Mutation of Gly256 to either a leucine or a phenylalanine yields the most dramatic effect on cavity volume. The G256L (Figure 7C) and G256F (Figure 7D) mutants have active site cavity volumes of 572 and 352 Å^3, respectively. The observed structural changes that reduce the volume of the active site cavity are consistent with the functional conversion from tetraketide synthesis by wild-type CHS and the G256A and G256V mutants to triketide formation by the G256L and G256F mutants.

DISCUSSION

Site-directed mutagenesis was used to replace Gly256 in the CHS elongation/cyclization cavity with alanine, valine, leucine, or phenylalanine residues. These mutations were used to establish the relationship between the size of the active site cavity and terminal chain lengths of resultant polyketide products. X-ray crystallographic and catalytic characterization of the G256A, G256V, G256L, and G256F mutants demonstrates that structural alterations in the active site cavity correlate with functional changes in the kinetic and specificity properties of each CHS mutant.

Regiospecific versus Nonspecific Cyclization of Tetraketide Intermediates in CHS. Following formation of a thioester-linked tetraketide from sequential condensation of *p*-coumaroyl-CoA and three malonyl-CoAs, wild-type CHS catalyzes an intramolecular Claisen condensation yielding chalcone (**1a**). In this step, the acidic methylene group (C6) nearest the coumaroyl moiety loses a proton with the resultant carbanion attacking the thioester carbonyl carbon (C1) (Figure 1) (*4*). Acridone synthase (*26*, *45*), homoeriodictyol/eriodictyol synthase (*25*), benzophenone synthase (*46*, *47*), valerophenone synthase (*48*), and 2,4-diacetylphloroglucinol synthase (*49*) catalyze identical regiospecific Claisen condensation reactions of the malonyl-derived portion of a tetraketide intermediate. Formation of these physiological products requires a defined conformation of the linear tetraketide intermediate for the cyclization reaction to proceed efficiently. Based on the three-dimensional structure of CHS, Ferrer et al. (*12*) proposed that the initiation/elongation/cyclization cavity serves as a structural template that selectively stabilizes a particular folded conformation of the linear tetraketide, allowing the Claisen condensation to proceed from C6 to C1 of the reaction intermediate. In contrast, CTAL (**1b**) formation can occur either in solution or alternatively while sequestered in the enzyme active site (*15*, *17*, *23*, *50*). In either case, enolization of the C5 ketone followed by nucleophilic attack on the C1 ketone with either a hydroxyl group (in solution) or the cysteine thiolate (enzyme bound) as the leaving group results in CTAL (**1b**). Similar lactones are commonly formed as byproducts of in vitro reactions in other PKS systems (*51*−*54*).

Structural changes within the elongation/cyclization pocket of CHS affect the ratio of Claisen-derived products versus lactone products with both physiological, i.e., *p*-coumaroyl-CoA, and nonphysiological starter molecules. The product profiles of the G256A and G256V mutants with *p*-coumaroyl-CoA (**1**) show an increase in the amount of CTAL (**1b**) produced versus the amount of naringenin formed, although the overall catalytic efficiency of each mutant is not dramatically altered. The three-dimensional structures of the G256A and G256V mutants exhibit small variations in the surface topology of the elongation cavity. While at first glance these changes appear insignificant, they most likely alter the conformation of the tetraketide intermediate enough to interfere with chalcone formation. Previous mutagenesis studies of CHS that demonstrate increased CTAL (**1b**) production also suggest that structural differences at other positions in the initiation/elongation/cyclization cavity alter the shape of the tetraketide intermediate (*15*, *55*). For example, mutation of Thr197 to a leucine in CHS causes a complete derailment of the normal tetraketide cyclization reaction, resulting in CTAL (**1b**) as the sole product (*15*). The current study establishes a direct link between structural changes in the active site cavity and functional differences in the cyclization reactions leading to chalcone (**1a**) and CTAL (**1b**) formation, respectively.

In reactions with alternate starter molecules, formation of a chalcone-like product also requires a regiospecific Claisen condensation reaction of the tetraketide intermediate (*44*).

Similar to the *Scutellaria* CHS (*31*), alfalfa CHS2 accepts phenylacetyl-CoA (**4**) and benzoyl-CoA (**5**) to catalyze formation of phlorobenzophenone (**5a**) and, less efficiently, the formation of phlorobenzyl ketone (**4a**). With both starter molecules, the G256A and G256V mutants again shift the chalcone-like product:tetraketide lactone product ratio. Interestingly, wild-type CHS, the G256A mutant, and the G256V mutant do not yield homoeriodictyol or phlorohexanyl ketone (**3a**) when feruloyl-CoA (**2**) or hexanoyl-CoA (**3**), respectively, are used as starter molecules. This indicates that larger starter molecules prevent the polyketide intermediate from adopting the conformation required for the regiospecific cyclization reaction. Similar results have been reported with 4-substituted analogues of *p*-coumaroyl-CoA (**1**) and other aliphatic starter molecules (*56*, *57*). Clearly, both the three-dimensional structure of the active site cavity and the shape and steric size of the substrate are crucial for optimally stabilizing the tetraketide intermediate's conformation that allows the regiospecific Claisen condensation reaction to proceed efficiently before derailment occurs.

Programming Polyketide Length: Tetraketide versus Triketide Formation in CHS. Triketide styrylpyrones are commonly found in fungi and occur as secondary metabolites in *Pinus strobus*, *Equisetum arvense*, and *Piper methylsticum* (*58*−*60*). Although there is no reported purification or cloning of an authentic styrylpyrone synthase, under certain in vitro reaction conditions wild-type CHS forms styrylpyrone products, suggesting this may be a vestigial activity in CHS family members. Originally, formation of *bis*-noryangonin (**1c**) from *p*-coumaroyl-CoA (**1**) and two malonyl-CoAs by CHS was reported as an artifact of high reductant concentrations in enzyme assays (*61*). Later experiments with aromatic starter molecules larger than *p*-coumaroyl-CoA (**1**), like feruloyl-CoA (**2**), showed that CHS yields triketide styrylpyrones in preference to chalcone-like products (*43*). Likewise, when *p*-coumaroyl analogues bearing a halogen in place of the hydroxyl group are used as the starter molecule, the corresponding styrylpyrones are formed (*57*). Also, use of phenylacetyl-CoA, hexanoyl-CoA, isovaleryl-CoA, and isobutyryl-CoA as starter molecules for *Pinus strobus* CHS produces triketide lactones in significant amounts (*56*). These experiments indicate that the choice of starter molecule alters both the regiochemistry of the cyclization reaction and the effective space available for complete extension of the polyketide intermediate, thus resulting in derailment of the reaction at the triketide step.

The results presented here demonstrate that replacement of Gly256 with larger amino acid residues causes a similar derailment. Since the CHS G256L and G256F mutants produce *bis*-noryangonin, our experiments demonstrate that a smaller active site cavity reduces the number of acetate additions made to the coumaroyl starter unit in a predictive manner from three to two, resulting in formation of a triketide product. Moreover, the G256L and G256F mutants yield mostly triketide lactone products with feruloyl-CoA (**2**), phenylacetyl-CoA (**4**), and benzoyl-CoA (**5**) starter molecules. Surprisingly, the G256L mutant still produces a tetraketide lactone (**3b**) with hexanoyl-CoA as a starter molecule. In this case, the increased flexibility of the hexanoyl moiety may permit accommodation of a tetraketide intermediate within the smaller active site cavity. Mechanistically, the lactonization reaction resulting in styrylpyrone is identical to that described above for CTAL (**1b**) formation. As discussed elsewhere (*15*), constricting the volume of the active site cavity near the elongation/cyclization lobe also influences starter molecule selectivity. For example, the G256L and G256F mutants consistently form the triketide methylpyrone in the presence of each alternate starter molecule. Both mutants catalyze the decarboxylation of malonyl-CoA to form acetyl-CoA, which serves as the starter molecule in these reactions that produce methylpyrone from three malonyl-CoA molecules.

Relationship to the Larger Family of CHS-like Enzymes. The overall backbone architecture of the CHS initiation/elongation/cyclization cavity, which is also structurally conserved in *Gerbera hybrida* 2-PS (*15*), is a versatile scaffold that natural selection has robustly exploited to generate an array of secondary metabolites in various plants and microorganisms (*3*). The sequence databases include nearly 400 CHS-related sequences from plants and microbes; however, the substrate and product specificities of many of the proteins encoded by these sequences remain undetermined.

The cloned and characterized CHS-like enzymes that form tetraketide products all have a glycine at position 256 (*16*−*26*). In comparison, the G256L mutation occurs naturally in *Gerbera hybrida* 2-PS, CHS-A, and CHS-B from various *Ipomoea* (morning glory) species, and *Petunia hybrida* CHS-B (*27*−*29*). 2-PS was originally annotated as a CHS. Later, Eckermann et al. (*27*) convincingly showed that it serves an alternate function in the biosynthesis of pyrone glucosides that contribute to insect and pathogen resistance in *Gerbera hybrida*. Currently, the metabolic role of the CHS variants in *Ipomoea* and *Petunia* remains to be established. CHS-G from *Petunia hybrida* (*28*) has an alanine at position 256; however, the function of this enzyme is also unresolved. Comparison of evolutionary rate variations between CHS-like enzymes suggests that *Ipomoea* CHS-A and CHS-B and *Petunia* CHS-B have acquired or are evolving new functions (*28*, *29*, *62*). Biochemical characterization of the *Ipomoea* and *Petunia* enzymes will likely demonstrate that these enzymes do not produce chalcones, but possibly function in the biosynthesis of other secondary metabolites, such as styrylpyrones.

Notably, natural variation in the type III PKS active site cavity like that observed in *Ipomoea* and *Petunia* does not result in functionally impaired enzymes but, in fact, generates catalytically active enzymes that display both altered substrate and product specificities. Sequential increases in the side chain volume of position 256 in alfalfa CHS2 result in decreases in polyketide chain length and predictable shifts in the ratio of tetraketide to triketide reaction products. These results functionally link the volume of the elongation/cyclization lobe in type III PKS to chain-length determination.

REFERENCES

1. Staunton, J., and Weissman, K. J. (2001) *Nat. Prod. Rep. 18*, 380−416.
2. Shen, B. (2000) *Top. Curr. Chem. 209*, 1−51.
3. Schröder, J. (1997) *Trends Plant Sci. 2*, 373−378.
4. Kreuzaler, F., and Hahlbrock, K. (1975) *Eur. J. Biochem. 56*, 205−213.
5. Tropf, S., Kärcher, B., Schröder, G., and Schröder, J. (1995) *J. Biol. Chem. 270*, 7922−7928.

6. Bailey, J. A., and Mansfield, J. W. (1982) *Phytoalexins*, John Wiley and Sons, New York.
7. Long, S. R. (1989) *Cell 56*, 203-214.
8. Dixon, R. A., and Paiva, N. L. (1995) *Plant Cell 7*, 1085−1097.
9. Lanz, T., Tropf, S., Marner, F.-J., Schröder, J., and Schröder, G. (1991) *J. Biol. Chem. 266*, 9971−9976.
10. Hahlbrock, K., Zilg, H., and Grisebach, H. (1970) *Eur. J. Biochem. 15*, 13−18.
11. Jez, J. M., Bowman, M. E., Dixon, R. A., and Noel, J. P. (2000) *Nat. Struct. Biol. 7*, 786−791.
12. Ferrer, J.-L., Jez, J. M., Bowman, M. E., Dixon, R. A., and Noel, J. P. (1999) *Nat. Struct. Biol. 6*, 775−784.
13. Jez, J. M., Ferrer, J.-L., Bowman, M. E., Dixon, R. A., and Noel, J. P. (2000) *Biochemistry 39*, 890−902.
14. Jez, J. M., and Noel, J. P. (2000) *J. Biol. Chem. 275*, 39640−39646.
15. Jez, J. M., Austin, M. B., Ferrer, J.-L., Bowman, M. E., Schröder, J., and Noel, J. P. (2000) *Chem. Biol. 7*, 919−930.
16. Schröder, J., Raiber, S., Berger, T., Schmidt, A., Schmidt, J., Soares-Sello, A. M., Bardshiri, E., Stack, D., Simpson, T. J., Veit, M., and Schröder, G. (1998) *Biochemistry 37*, 8417−8425.
17. Shiokawa, K., Inagaki, Y., Morita, H., Hsu, T.-J., Iida, S., and Noguchi, H. (2000) *Plant Biotechnol. 17*, 203−210.
18. Batschauer, A., Ehmann, B., and Schafer, E. (1991) *Plant Mol. Biol. 16*, 175−185.
19. Nakajima, O., Akiyama, T., Hakamatsuka, T., Shibuya, M., Noguchi, H., Ebizuka, Y., and Sankawa, U. (1991) *Chem. Pharm. Bull. 39*, 1911−1913.
20. Fliegmann, J., Schröder, G., Schanz, S., Britsch, L., and Schröder, J. (1992) *Plant Mol. Biol. 18*, 489−503.
21. Schröder, G., Brown, J. W., and Schröder, J. (1988) *Eur. J. Biochem. 172*, 161−169.
22. Melchior, F., and Kindl, H. (1990) *FEBS Lett. 268*, 17−20.
23. Akiyama, T., Shibuya, M., Liu, H.-M., and Ebizuka, Y. (1999) *Eur. J. Biochem. 263*, 834−839.
24. Reinecke, T., and Kindl, H. (1993) *Phytochemistry 35*, 63−66.
25. Christensen, A. B., Gregersen, P. L., Schröder, J., and Collinge, D. B. (1998) *Plant Mol. Biol. 37*, 849−857.
26. Junghanns, K. T., Kneusel, R. E., Baumert, A., Maier, W., Groger, D., and Matern, U. (1995) *Plant Mol. Biol. 27*, 681−692.
27. Eckermann, S., Schröder, G., Schmidt, J., Strack, D., Edrada, R. A., Helariutta, Y., Elomaa, P., Kotilainen, M., Kilpeläinen, I., Proksch, P., Teeri, T. H., and Schröder, J. (1998) *Nature 396*, 387−390.
28. Koes, R. E., Spelt, C. E., van den Elzen, P. J. M., and Mol, J. N. M. (1989) *Gene 81*, 245−257.
29. Durbin, M. L., Learn, G. H., Huttley, G. A., and Clegg, M. T. (1995) *Proc. Natl. Acad. Sci. U.S.A. 92*, 3338−3343.
30. Stoeckigt, J., and Zenk, M. H. (1975) *Z. Naturforsch. 30C*, 352−358.
31. Morita, H., Takahashi, Y., Noguchi, H., and Abe, I. (2000) *Biochem. Biophys. Res. Commun. 279*, 190−195.
32. Otwinowski, Z., and Minor, W. (1997) *Methods Enzymol. 276*, 307−326.
33. Collaborative Computational Project 4 (CCP4) (1994) *Acta Crystallogr. D50*, 760−763.
34. Ten Eyck, L. F. (1973) *Acta Crystallogr. A29*, 183−191.
35. Ten Eyck, L. F. (1977) *Acta Crystallogr. A33*, 486−492.
36. Murshudov, G. N., Vagin, A. A., and Dodson, E. J. (1997) *Acta Crystallogr. D53*, 240−255.
37. Lamzin, V. S., and Wilson, K. S. (1993) *Acta Crystallogr. D49*, 129−147.
38. Jones, T. A., Zou, J. Y., Cowan, S. W., and Kjeldgaard, M. (1993) *Acta Crystallogr. D49*, 148−157.
39. Laskowski, R. A., MacArthur, M. W., Moss, D. S., and Thornton, J. M. (1993) *J. Appl. Crystallogr. 26*, 283−291.
40. Nicholls, A., Sharp, K., and Honig, B. (1991) *Proteins: Struct., Funct., Genet. 11*, 281−296.
41. Kraulis, P. J. (1991) *J. Appl. Crystallogr. 24*, 946−950.
42. POV−Team (1997) *POV−Ray: persistence of vision raytracer*. http://www.povray.org.
43. Hrazdina, G., Kreuzaler, F., Hahlbrock, K., and Grisebach, H. (1976) *Arch. Biochem. Biophys. 175*, 392−399.
44. Schüz, R., Heller, R., and Hahlbrock, K. (1983) *J. Biol. Chem. 258*, 6730−6734.
45. Lukacin, R., Urbanke, C., Groning, I., and Matern, U. (1999) *FEBS Lett. 448*, 135−140.
46. Beerhues, L. (1996) *FEBS Lett. 383*, 264−266.
47. Schmidt, W., and Beerhues, L. (1997) *FEBS Lett. 420*, 143−146.
48. Paniego, N. B., Zuurbier, K. W. M., Fung, S.-Y., van der Heijden, R., Scheffer, J. C. C., and Verpoorte, R. (1999) *Eur. J. Biochem. 262*, 612−616.
49. Bangera, M. G., and Thomashow, L. S. (1999) *J. Bacteriol. 181*, 3155−3163.
50. Yamaguichi, T., Kurosaki, F., Suh, D.-Y., Sankawa, U., Nishioka, M., Akiyama, T., Shibuya, M., and Ebizuka, Y. (1999) *FEBS Lett. 460*, 457−461.
51. Dimroth, P., Walter, H., and Lynen, F. (1970) *Eur. J. Biochem. 13*, 98−110
52. Spencer, J. B., and Jordan, P. M. (1992) *Biochem. J. 288*, 839−846
53. Schorr, R., Mittag, M., Müller, G., and Schweizer, E. (1994) *Plant Physiol. 143*, 407−415
54. Kurosaki, F., Kizawa, Y., and Nishi, A. (1989) *Eur. J. Biochem. 185*, 85−89.
55. Suh, D.-Y., Fukuma, K., Kagami, J., Yamazaki, Y., Shibuya, M., Ebizuka, Y., and Sankawa, U. (2000) *Biochem. J. 350*, 229−235.
56. Zuubier, K. W. M., Leser, J., Berger, T., Hofte, A. J. P., Schröder, G., Verpoorte R., and Schröder, J. (1998) *Phytochemistry 49*, 1945−1951.
57. Abe, I., Morita, H., Nomura, A., and Noguchi, H. (2000) *J. Am. Chem. Soc. 122*, 11242−11243.
58. Schröder, J. (1999) in *Comprehensive Natural Products Chemistry* (Barton, D., Nakanishi, K., Meth-Cohn, O., and Sankawa, U., Eds.) pp 749−771, Elsevier Press, Amsterdam, The Netherlands.
59. Beckert, C., Horn, C., Schnitzler, J.-P., Lehning, A., Heller, W., and Veit, M. (1997) *Phytochemistry 44*, 275−283.
60. Briskin, D. P. (2000) *Plant Physiol. 124*, 507−514.
61. Kreuzaler, F., and Hahlbrock, F. (1975) *Arch. Biochem. Biophys. 169*, 84−90.
62. Rausher, M. D., Miller, R. E., and Tiffin, P. (1999) *Mol. Biol. Evol. 16*, 266−274.

BI015621Z